Accepted in ACS Omega on 17th December 2021

Clay swelling: role of cations in stabilizing/destabilizing mechanisms

Wen L. Chen[a], Robert C. Grabowski[a] and Saurav Goel[b,c,d]*

[a]School of Water, Energy and Environment, Cranfield University, Cranfield, Bedfordshire MK43 0AL, UK.

[b] London South Bank University, London SE1 0AA, UK.

[c] Indian Institute of Technology Guwahati, Guwahati, 781039, India

[d] University of Petroleum and Energy Studies, Dehradun, 248007, India

ABSTRACT

The stepwise hydration of clay minerals has been observed repeatedly in studies, but the underlying mechanism remains unclear. Previous numerical studies confirmed the existence of one water layer (1W) and two water layer (2W) hydration states. However, the undisturbed transition in between these hydration states has never been captured. Using molecular dynamics simulation, this study (i) simulated for the first time the free 1W-2W transition during clay hydration and (ii) identified the underlying mechanism to be the detachment of cations from the

clay surface and the formation of a shell of water molecules around the cation. The swelling dynamics of clay was found to be affected by the clay charge, clay minerology and counter ions through complex cation-clay interactions, cation hydration capacity and cation migration rate.

Introduction

Clays, such as montmorillonite (MMT) and beidellite (BD), are important constituents of soil and have wide engineering applications, including building material, environmental remediation, catalysis, and geological disposal of nuclear waste [1–4]. MMT and BD carry negative charges in their plate-like layers, due to the isomorphous substitution of silicon (Si) or aluminum (Al) atoms with atoms of lower valence. To balance out the charge, these substitutions are associated with positively charged cations within the interlayer space [5]. In the presence of water, the interlayer cations attract water molecules, pushing clay layers apart, in a process generally described as clay hydration or clay swelling [6,7]. However, questions remain on the molecular dynamics driving clay swelling, particularly related to the molecular interactions that affect the movement of cation and water molecules in the inter-particle layer of expansive clays.

Clay swelling occurs in two regimes, crystalline and osmotic, depending on the *d-space* of the clay particle. The *d-space* is defined for clay particles as the sum of the interlayer distance and the thickness of one clay layer. Crystalline swell*ing* occurs when the *d-space* increases from 10 Å to 22 Å, and osmotic swell*ing* when *d-space* swells beyond 22 Å [8]. Crystalline swell*ing* has been observed to occur in a stepwise fashion [9]. The *d-space* changes abruptly from dry to a one water layer (1W) hydration state, and from a one water layer to two water layer (2W) hydration state [8–10]. Numerical simulations have been performed to investigate aspects of the hydration process of clay [9–18]. However, previous studies have either (i) inserted water molecules into the

space confined by clay layers infinitely extending in horizontal directions, [7,16,19–21]; (ii) steered molecular dynamics by imposing extra expanding force or potential [12,18]; or (iii) focused on swelling dynamics at a larger *d-space* (i.e., 18.8 Å in [11]). There remain significant gaps in our scientific understanding of (i) 'free' swell from the 1W to 2W hydration states, in which water molecules are allowed to move freely from bulk water to the interlayer space, (ii) the underlying molecular mechanism of stepwise swell, and (iii) the influence of clay charge, mineralogy and interlayer cations on the 'free' swell of clays. To address these gaps, molecular dynamics simulation on the swell of clay particle was performed in this study.

Materials and Methods

Recent development in the CLAYFF force field allows clay particles in a molecular dynamics simulation (LAMMPS [22]) to have protonated edges [12,14,23,24]. With CLAYFF, water molecules can move freely in and out of the clay particle, something that was not possible in earlier force-fields[15,25]. In this study, the mechanisms underlying stepwise swell were investigated using a two-layer model placed in a water box (Fig. S1 in supporting information). Each layer was modelled as a Tetrahedral-Octahedral-Tetrahedral (T-O-T) structure contained 8 $Si_8(Al_{4-x}Mg_x)O_{20}(OH)_4$ (representing MMT) or $Si_{8-x}Al_{4+x}O_{20}(OH)_4$ (representing BD) units. x substitution of O-Al by Mg (Magnesium) in MMT or T-Si by Al in BD leads to a $-x$ e/unit cell charge. Sodium (Na), potassium (K) and calcium (Ca) were chosen as counter ions for their differences in valence and hydration capacity[26]. The simulations were directed to test the effect of clay charge (from -0.125 to -0.75 e/unit *cell*), using different numbers of Na counter ions (2, 4, 6, 8, 10 and 12 ions), and cation types (K and Ca, with 12 and 6 ions, respectively). The bottom layer was kept fixed throughout the simulation [13,27]. The top layer was fixed for the first 1 ns of simulation to allow the system to reach equilibrium, and then was allowed to move freely

vertically in which case the clay swells naturally. No other restriction was applied to the system (preparation of clay sample and model system are provided as supporting information).

Results and Discussion

Relaxing from an initial *d-space* of 11.9 Å, stable hydration states and stepwise swell were successfully reproduced for MMT (Fig. 1). Stable 1W states were observed for Na with 2 and 4 counter ions in the interlayer space (Fig. 1a, b) and for K with 12 counter ions (Fig. 1g). Stepwise swell from 1W to 2W state was observed for Na, with 10 and 12 counter ions (Fig. 1e, f) and Ca with 6 counter ions (Fig. 1h). There was no evidence of stable, higher hydration states. In simulations relaxed from higher initial *d-space*, i.e., at 15.8 Å and 18.8 Å, Ca6 reached a stable 2W state for both initial *d-spaces*, and Na12 reached a stable 2W state at a 15.8 Å initial *d-space* (Fig. S4*5* in supporting information). The 1W hydration state of Na8 and Ca6 were very short, indicating a direct swell to the 2W hydration state. Continued osmotic swelling was observed for Na with 6, 8 and 10 counter ions. The 1W-2W swell occurs rapidly, i.e., in less than 0.2 ns, leading to a sudden change in the measured d-space, which is distinct from the continuous change in d-space in osmotic swelling (i.e., in Na6, Na8 and Na10). The *d-space* of 1W and 2W hydration states agree well with experimental observation and previous numerical studies (Fig.1) [11,18,28–33]. In particular, the 1W and 2W *d-space* of Na12 aligns closely with prior molecular simulation studies (Fig. 1f), i.e., 12.57 Å for 1W and 15.03 Å for 2W[12]. The simulations reproduce previously observed swelling behaviors of Na-MMT [34], specifically the expansion to 2W and the higher *d-space* for Na-MMT of medium and high charge (Fig. 1c, d, e and f).

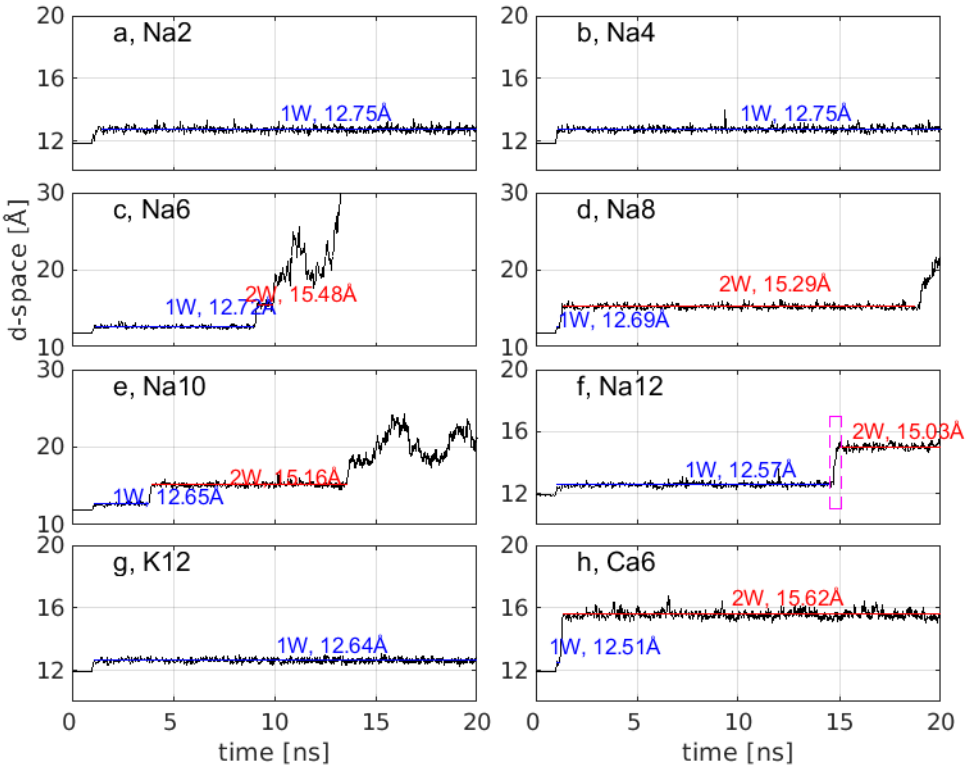

Figure 1. Hydration of MMT over time as represented by d-space: a, Na2, with 2 Na in the interlayer space, carries -0.125 e/unit cell; b, Na4, carries -0.25 e/unit cell; c, Na6, carries -0.375 e/unit cell; d, Na8, carries -0.5 e/unit cell; e, Na10, carries -0.625 e/unit cell; f, Na12, carries -0.75 e/unit cell; g, K12, carries -0.75 e/unit cell; and h, Ca6, carries -0.75 e/unit cell.

The simulations indicate that the mechanism of crystalline swell*ing* is the detachment and hydration of the counter ions. The coordination of water oxygen (O_w) with counter ions was observed to begin before the abrupt increase in the *d-space* and continued during the swelling process, along with a decrease in the number of coordinated clay oxygen (O_b, Fig. 2b). O_w and O_b within a 3.0 Å zone from the counter ion were coordinated. Visualization of the atomic interactions illustrates that during crystalline swell*ing* the top O_b and top layer are pushed upward as the bond between Na and O_b breaks and a new bond between Na and O_w forms (Fig.

2a). As a result, the density profile of O_w splits from one peak around Na at 1W state to two peaks around Na at 2W state (Fig. 2c, d, e). Correlation analysis of *d-space* and averaged coordinated O_w and O_b (i.e., total number of coordinated O_w or O_b divided by the number of interlayer cations), collected at the 1W-2W transition, confirms the high correlation between these data sets (Fig. 3). A shell of four O_w and two O_b surrounds a single Na at 1W state and a shell of six O_w at 2W state. The same correlation was found for the 1W-2W transition for Na6, Na8, Na10 and Ca6 (not presented here), which supports previous studies reporting the influence of interlayer cation hydration on the crystalline swell*ing* of clay [6,15,17,19].

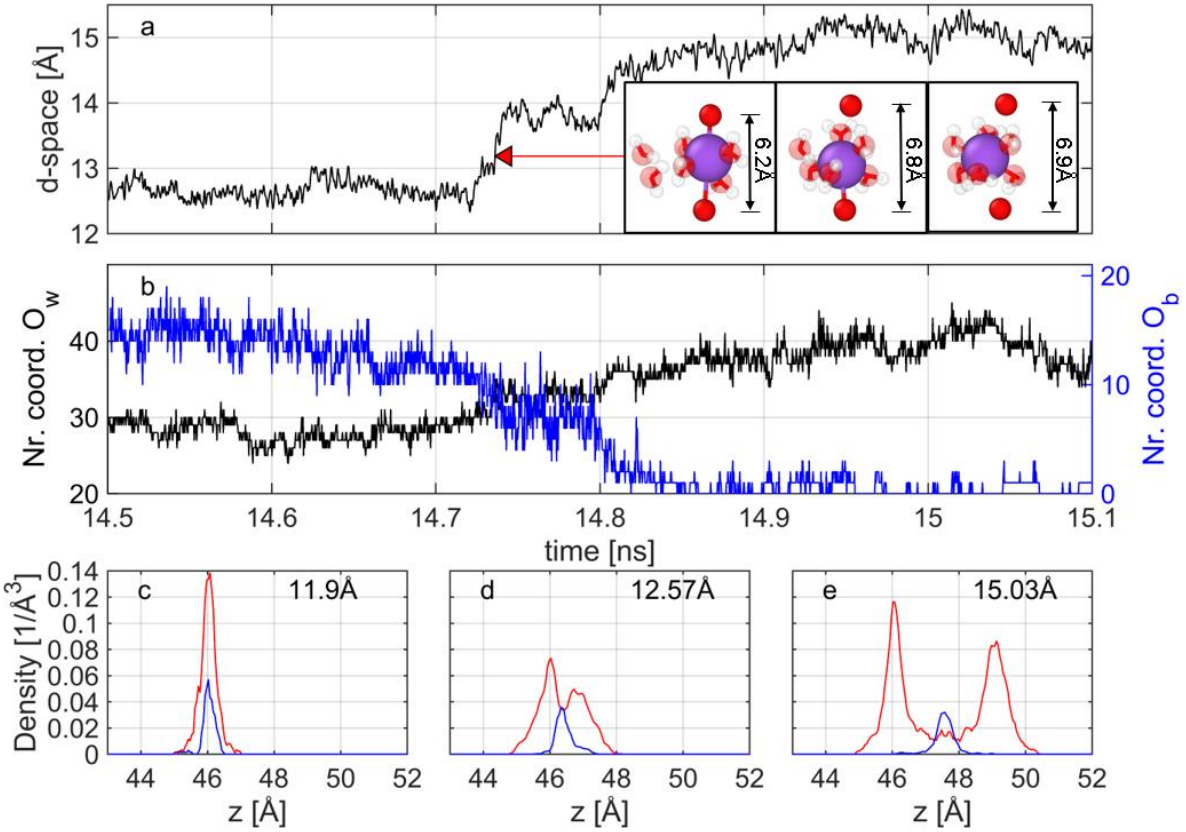

Figure 2. Detailed 1W-2W swell process of Na12 (the magenta rectangle in Fig. 1f): a, the evolution of *d-space*; and b, the evolution of coordinated O_w (black curve) and O_b (blue curve) number. Distribution of O_w (red curve) and Na (blue curve) within the interlayer space at *d-space*

of c, 11.9 A; d, 12.57 A (1W); and e, 15.03 A (2W) are present. The slightly lower peaks at higher z position in d and e are due to the fluctuation of top layer.

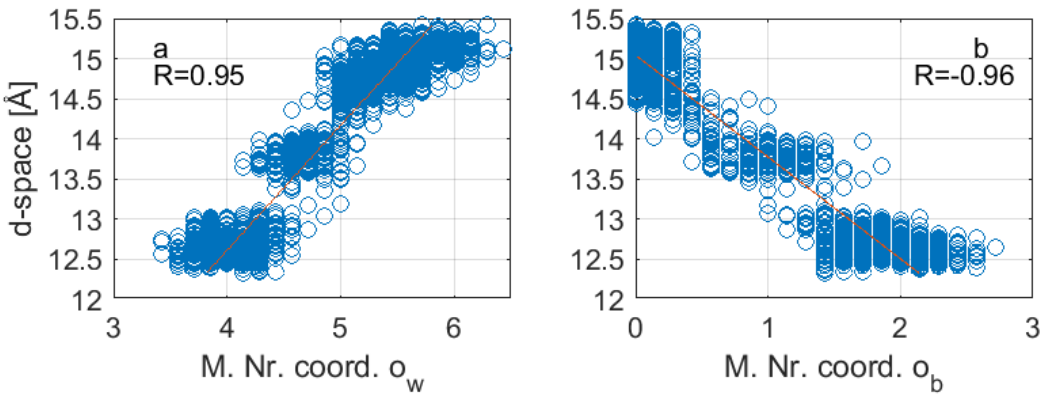

Figure 3. Correlation between *d-space* and the average number of coordinated O_w (a) and O_b (b) for each cation for MMT.

Whilst the hydration of counter ions is the mechanism generating crystalline swell*ing*, the counter ions are still responsible for the dominant attractive force stabilizing the 1W and 2W hydration states. An analysis of the force imposed on the top clay layer identifies an attractive force ($F_{TC}<0$) from the interlayer cations, which has a greater magnitude than the repulsive force from the bottom layer ($F_{TB}>0$ and $|F_{TC}|>|F_{TB}|$) (Fig. 4a, b). A third force stems from the interaction between the top clay layer and the surrounding water molecules, which can be either repulsive or attractive depending on their relative location. The water molecules within the interlayer space, however, always provide strong repulsive force on the top clay layer ($F_{TW}>0$, Fig. 4a, b). In the process of 1W-2W swell, water molecules are attracted to coordinate with the interlayer cations. As a result, F_{TW} continuously increases and pushes up the top clay layer (Fig. S2 in supporting information). The decomposition of these forces shows that, in the first two forces, the coulombic interaction dominates over pair-wise interactions, whereas in the third

force only pair-wise interaction is involved (Fig.S3 in supporting information). The swelling state of clay particle depends on the competition between these three contributions.

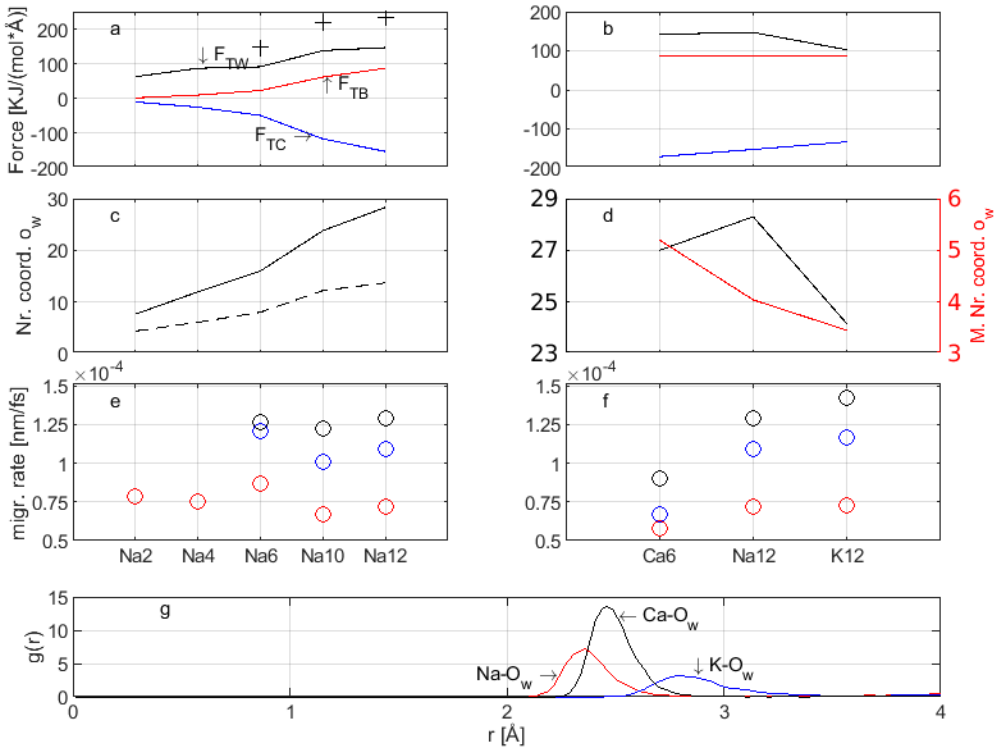

Figure 4. Force analysis showing: a, forces on top clay layer for Na-MMT with various clay charge, black crosses stand for F_{TW} at 2W state, negative/positive value indicates an attractive/repulsive force on the top layer; b, forces on top layer for Ca-, Na- and K-MMT with 6, 12 and 12 counter ions; c, total coordinated O_w for interlayer Na, black dashed curve indicates the missing number of O_w to be attracted if all Na are fully hydrated; d, total (black) and mean (red) number of coordinated O_w for Ca, Na and K extracted at 1W hydration state; e, migration rates of interlayer Na, with red, blue and black color distinguishing cation in interlayer region, 1 nm away from clay and bulk water; f, migration rates for interlayer Na, Ca and K; g, the *r*adial

distribution function of cation and O_w. All results presented were extracted from 1W hydration states unless specified.

Clay with a higher negative charge (i.e., greater number of substitutions) experiences stronger repulsive/attractive force from the bottom clay/cation, but also stronger repulsive force from the hydration of interlayer Na (Fig. 4a). The full hydration of Na attracted six O_w to form a shell surrounding one single Na (Fig. 3). The strong repulsive force exerted on the top layer in this process is indicated by the number of missing coordinated O_w. At 1W hydration state, the repulsive force increases for clay of higher negative charge (Fig. 4c), as more interlayer Na attract water and become fully hydrated. As a result, the equilibrium state of the Na6, Na8, Na10 and Na12 swelled beyond 1W hydration state. A smaller 1W d-space was observed for clay of higher negative charge (Fig. 1), which agrees with experimental observation and is due to a stronger clay cation attraction [35]. At 2W state, the stronger clay cation interaction in the Na12 constrained a 2W state *(Fig. 5)*, whereas Na6 Na8 and Na10 continued to swell. For Na10, the diffusion of Na from interlayer region to bulk water leads to weaker constraining forces from cation to both top and bottom clay layers (Fig. 5a-c), which in turn reduces the resistance to the migration of water molecules into the interlayer region (i.e., driven by the osmotic pressure) and the osmotic swelling of clay. Alternatively, the stronger force and interaction between clay and cation in Na12 restrains Na from moving out of the interlayer region and prevents osmotic swelling, as suggested by previous experimental studies[26]. The various hydration states of medium charged clay and high charged clay result from the competition between osmotic pressure and cation-clay interaction, which requires further molecular dynamic studies to verify.

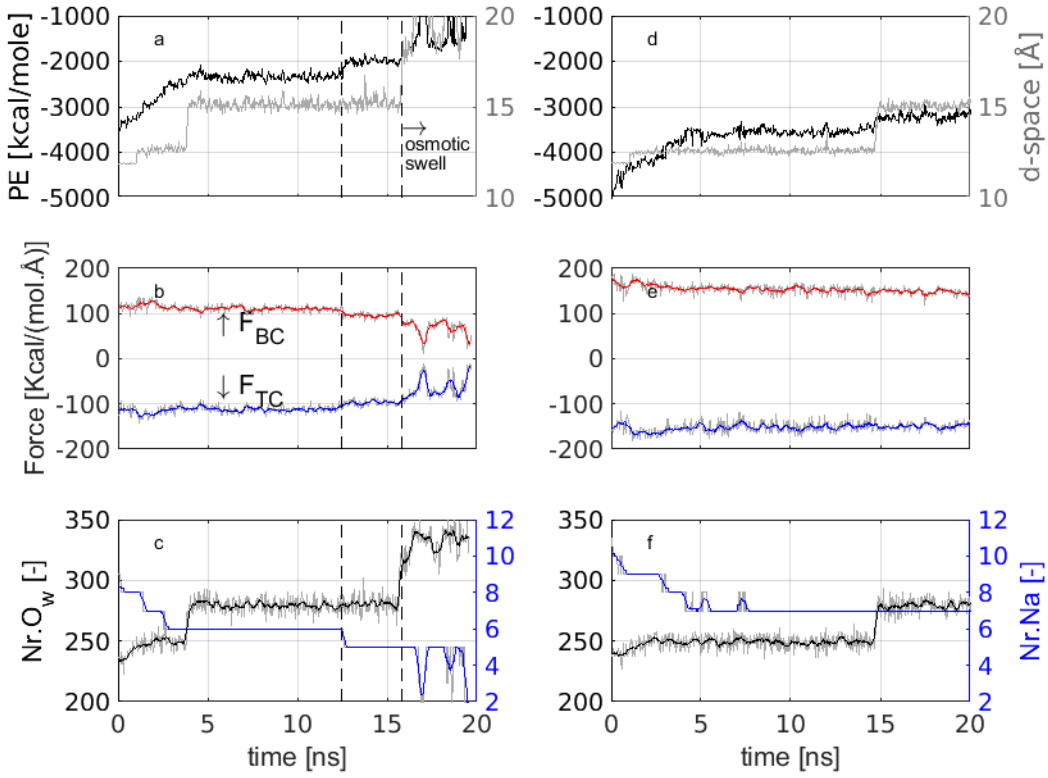

Figure 5. Comparison of swelling for Na10 (a-c) and Na12 (d-f), showing: a, the interaction energy of clay and interlayer cation (black) and swelling curve (grey); b, forces from interlayer cation onto the top clay layer (F_{TC}, red) and the bottom clay layer (F_{BC}, blue); c, number of interlayer O_w (black) and Na (blue).

In addition to the hydration capacity of the cation, the swelling behavior of Na-, K-, and Ca-MMT varies due to the mobility of the counter ion in the interlayer space. The number of coordinated O_w attracted to the cations at its 1W state differs between Ca, Na and K (Fig. 4d), indicating a decreasing hydration capacity [17]. This behavior is supported by the radial distribution function of cations and O_w (Fig. 4g). Ca had the greatest density of coordinated O_w, and K the lowest, with Na intermediate. The migration of cations (depending on the type of cation) within the interlayer space is greatly inhibited by the clay (Fig. 4e, f). Among these cations, the inhibition effect is strongest on K, as its migration rate drops most from the bulk

water environment to interlayer space [36]. As a combined result of weak hydration capacity and strong inhibition on migration, K-MMT had the most stable 1W hydration state (Fig. 1g) [33]. The strong hydration capacity of Ca led to a quick swell of Ca-MMT to 2W state (Fig. 1h), whereas its low migration rate prevented it from swelling to higher *d-space* (Fig.S4*5*c)[19]. The intermediate hydration capacity of Na led to the slow 1W-2W transition of Na12 (Fig. 1f), but at higher *d-space* the stabilizing effect of Na was weakened by its fast migration rate (i.e., osmotic swell*ing* of Na12 when relaxed from 18.8 Å).

The hydration of Na-BD relaxed from 11.9 Å *d-space* reached stable 1W states for all charges (Fig. 6*a-d*). The 1W *d-space* of BD (i.e., 13.04 Å and 13.1 Å for BD-Na4 and BD-Na12, Fig.6) were larger than that of MMT (i.e., 12.75 Å and 12.57 Å for Na4 and Na12, Fig.1). In contrast, the 2W *d-space* of BD generated with higher initial *d-space* were smaller, i.e., around 14.3 Å for BD (Fig. S4*5*d, e) compared with above 15.0 Å for MMT (Fig. 1c-f and Fig. S4*5*a-c). This reverse in the trend has also been observed by a previous modelling study [15] and supported by experimental work [37]. Compared to MMT, F_{TB} and F_{TC} were stronger in BD and the interlayer Na migration rate was lower (Fig. 6f), which is due to the shift from central negative charge in MMT (as O-Al replaced by Mg) to a surface negative charge in BD (as T-Si replaced by Al). The interlayer Na density profile of BD was flat and loosely split into two peaks, in contrast to a single peak profile in MMT, indicating that Na in BD is more attracted to the clay surface (Fig. 6h). BD with 12 K and 6 Ca as counter ions also stabilizes at 1W states (Fig. S4).

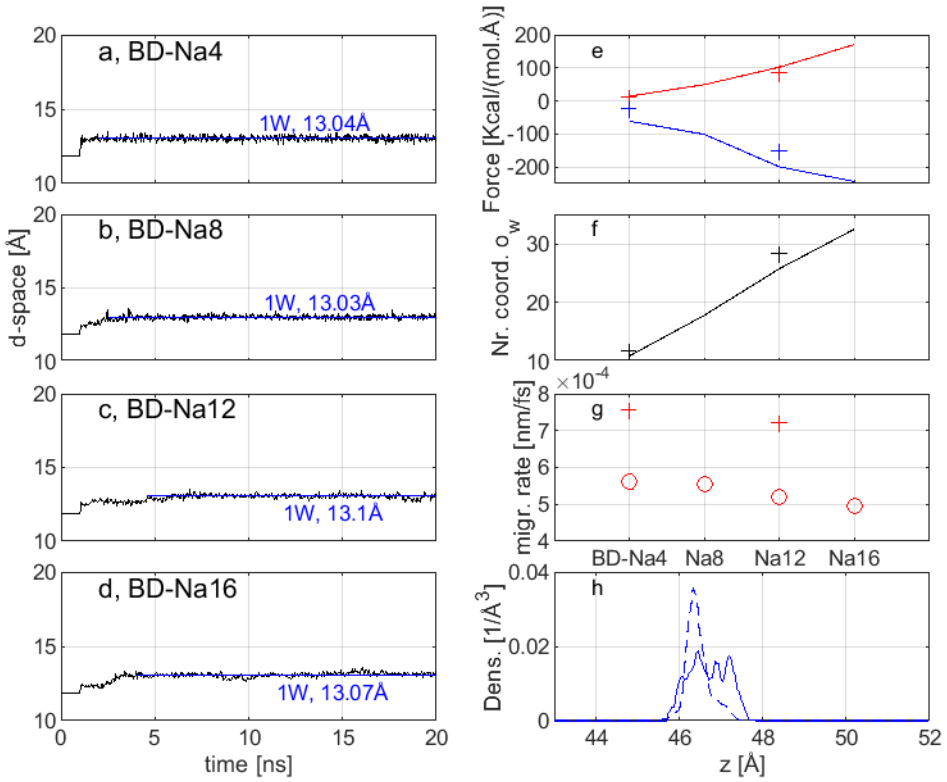

Figure 6. Swelling of BD showing: a, the swelling curve of BD-Na4, with 4 Na as counter ions and carries -0.25 e/unit cell charge; b, swelling curve of BD-Na8, carries -0.5 e/unit cell; c, swelling curve of BD-Na12, carries -0.75 e/unit cell; and d, swelling curve of BD-Na16, carries -1.0 e/unit cell; *e,* forces on top clay for F_{TB} (red) and F_{TC} (blue); f, the number of coordinated interlayer O_w*; g,* the migration rate of interlayer Na; h, the density profile of interlayer Na for Na12 in BD (solid) and MMT (dashed). Crosses in e, f and g are values for MMT.

In this study, free swell was investigated from the 1W hydration state, not 0W, because of the existence of an energy barrier for 0W-1W swell [12,18]. At 1W and higher d-space, the protonated clay edge permits the diffuse of water molecules and cations, but, at 0W state, exposed -OH groups form hydrogen bonds in between adjacent layers. According to Ho et al.[12], these hydrogen bonds act like a gate preventing the inflow of water molecules into the interlayer space

and imposes an energy barrier for 0W-1W swell. Consequently, simulation with the current CLAYFF is not able to simulate the 0W-1W swell. Fixing the bottom layer and controlling the direction of swell have been used to estimate the osmotic swelling pressure of clay [13,27], and are firstly used to investigate the free 1W-2W swell in this study. It is a stepwise improvement in the modelling. Future modelling should consider the lateral movement of the clay layers, and the breakdown or misorientation of clay platelets in the swelling process, which has been observed in the swelling experiment and is found to affect the interlayer water content [38].

Conclusions

Using a molecular dynamics approach, this study simulated the free expansion of clay layers during hydration and identified the key mechanisms for the stepwise swell from a 1W to 2W hydration state. Crystalline swell*ing* is triggered by the detachment of cations from the clay surface and the formation of a shell of water molecules around the cations in the interlayer space. The full hydration of cations causes the clay to swell from a 1W to 2W hydration state, but it also generates the attractive force that stabilizes both states through clay-cation coulombic attraction. Importantly, the swelling dynamics of clay is affected by the clay charge, clay minerology and counter ions through complex cation-clay interactions, cation hydration capacity and cation migration rate. Future work should investigate the chemistry and interactions of the surrounding water with the counter ion and its effect on clay swelling.

Notes

The authors declare no competing financial interests.

ACKNOWLEDGMENT

This work was supported primarily by the Engineering and Physical Science Research Council (Grant number EP/T001100/1). S. Goel also acknowledges support from other EPSRC grants (EP/L016567/1, EP/S013652/1, EP/S036180/1, and EP/T024607/1), the Royal Academy of Engineering via Grants No. IAPP18-19\295, TSP1332 and EXPP2021\1\277, EURAMET EMPIR A185 (2018), EU Cost Action (CA15102, CA18125, CA18224 and CA16235), Newton Fellowship award from the Royal Society (NIF\R1\191571), and the European Regional Development Funds (ERDF) sponsored A2i project at LSBU that have catalysed several industrial partnerships. The research made use of Isambard Bristol, UK supercomputing service accessed by Resource Allocation Panel (RAP) grant as well as ARCHER2 resources (Project e648).

ASSOCIATED CONTENT

Supporting information is available free of charge on the ACS Publication website

REFERENCES

(1) Amato, I. Green Cement: Concrete Solutions. *Nature* **2013**, *494* (7437), 300–301. https://doi.org/10.1038/494300a.

(2) Carretero, M. I.; Pozo, M. Clay and Non-Clay Minerals in the Pharmaceutical and Cosmetic Industries Part II. Active Ingredients. *Applied Clay Science* **2010**, *47* (3), 171–181. https://doi.org/https://doi.org/10.1016/j.clay.2009.10.016.

(3) Carretero, M. I. Clay Minerals and Their Beneficial Effects upon Human Health. A Review. *Applied Clay Science* **2002**, *21* (3), 155–163. https://doi.org/https://doi.org/10.1016/S0169-1317(01)00085-0.

(4) Wu, L. M.; Zhou, C. H.; Keeling, J.; Tong, D. S.; Yu, W. H. Towards an Understanding of the Role of Clay Minerals in Crude Oil Formation, Migration and Accumulation. *Earth-Science Reviews* **2012**, *115* (4), 373–386. https://doi.org/https://doi.org/10.1016/j.earscirev.2012.10.001.

(5) Suter, J. L.; Anderson, R. L.; Christopher Greenwell, H.; Coveney, P. v. Recent Advances in Large-Scale Atomistic and Coarse-Grained Molecular Dynamics Simulation of Clay

Minerals. *Journal of Materials Chemistry* **2009**, *19* (17), 2482–2493. https://doi.org/10.1039/b820445d.

(6) Zhou, Z. Construction and Application of Clay-Swelling Diagrams by Use of XRD Methods. *Journal of Petroleum Technology* **1995**, *47* (04), 306. https://doi.org/10.2118/29224-PA.

(7) Hensen, E. J. M.; Smit, B. Why Clays Swell. *Journal of Physical Chemistry B* **2002**, *106* (49), 12664–12667. https://doi.org/10.1021/jp0264883.

(8) Rao, S. M.; Thyagaraj, T.; Raghuveer Rao, P. Crystalline and Osmotic Swelling of an Expansive Clay Inundated with Sodium Chloride Solutions. *Geotechnical and Geological Engineering* **2013**, *31* (4), 1399–1404. https://doi.org/10.1007/s10706-013-9629-3.

(9) Meleshyn, A.; Bunnenberg, C. The Gap between Crystalline and Osmotic Swelling of Na-Montmorillonite: A Monte Carlo Study. *Journal of Chemical Physics* **2005**, *122* (3). https://doi.org/10.1063/1.1834499.

(10) Chávez-Páez, M.; dePablo, L.; dePablo, J. J. Monte Carlo Simulations of Ca–Montmorillonite Hydrates. *The Journal of Chemical Physics* **2001**, *114* (24), 10948–10953. https://doi.org/10.1063/1.1374536.

(11) Hsiao, Y. W.; Hedström, M. Swelling Pressure in Systems with Na-Montmorillonite and Neutral Surfaces: A Molecular Dynamics Study. *Journal of Physical Chemistry C* **2017**, *121* (47), 26414–26423. https://doi.org/10.1021/acs.jpcc.7b09496.

(12) Ho, T. A.; Criscenti, L. J.; Greathouse, J. A. Revealing Transition States during the Hydration of Clay Minerals. *Journal of Physical Chemistry Letters* **2019**, *10* (13), 3704–3709. https://doi.org/10.1021/acs.jpclett.9b01565.

(13) Sun, L.; Hirvi, J. T.; Schatz, T.; Kasa, S.; Pakkanen, T. A. Estimation of Montmorillonite Swelling Pressure: A Molecular Dynamics Approach. *Journal of Physical Chemistry C* **2015**, *119* (34), 19863–19868. https://doi.org/10.1021/acs.jpcc.5b04972.

(14) Cygan, R. T.; Greathouse, J. A.; Heinz, H.; Kalinichev, A. G. Molecular Models and Simulations of Layered Materials. *Journal of Materials Chemistry* **2009**, *19* (17), 2470–2481. https://doi.org/10.1039/b819076c.

(15) Teich-McGoldrick, S. L.; Greathouse, J. A.; Jové-Colón, C. F.; Cygan, R. T. Swelling Properties of Montmorillonite and Beidellite Clay Minerals from Molecular Simulation: Comparison of Temperature, Interlayer Cation, and Charge Location Effects. *Journal of Physical Chemistry C* **2015**, *119* (36), 20880–20891. https://doi.org/10.1021/acs.jpcc.5b03253.

(16) Segad, M.; Jönsson, B.; Åkesson, T.; Cabane, B. Ca/Na Montmorillonite: Structure, Forces and Swelling Properties. *Langmuir* **2010**, *26* (8), 5782–5790. https://doi.org/10.1021/la9036293.

(17) Rahromostaqim, M.; Sahimi, M. Molecular Dynamics Simulation of Hydration and Swelling of Mixed-Layer Clays. *Journal of Physical Chemistry C* **2018**, *122* (26), 14631–14639. https://doi.org/10.1021/acs.jpcc.8b03693.

(18) Shen, X.; Bourg, I. C. Molecular Dynamics Simulations of the Colloidal Interaction between Smectite Clay Nanoparticles in Liquid Water. *Journal of Colloid and Interface Science* **2020**, *584*, 610–621. https://doi.org/10.1016/j.jcis.2020.10.029.

(19) Zhang, L.; Lu, X.; Liu, X.; Zhou, J.; Zhou, H. Hydration and Mobility of Interlayer Ions of (Nax, Cay)-Montmorillonite: A Molecular Dynamics Study. *Journal of Physical Chemistry C* **2014**, *118* (51), 29811–29821. https://doi.org/10.1021/jp508427c.

(20) Yang, Y.; Narayanan Nair, A. K.; Sun, S. Layer Charge Effects on Adsorption and Diffusion of Water and Ions in Interlayers and on External Surfaces of Montmorillonite. *ACS Earth and Space Chemistry* **2019**, *3* (11), 2635–2645. https://doi.org/10.1021/acsearthspacechem.9b00236.

(21) Li, Y.; Narayanan Nair, A. K.; Kadoura, A.; Yang, Y.; Sun, S. Molecular Simulation Study of Montmorillonite in Contact with Water. *Industrial & Engineering Chemistry Research* **2019**, *58* (3), 1396–1403. https://doi.org/10.1021/acs.iecr.8b05125.

(22) Plimpton, S. Fast Parallel Algorithms for Short-Range Molecular Dynamics. *Journal of Computational Physics* **1995**, *117* (1), 1–19. https://doi.org/https://doi.org/10.1006/jcph.1995.1039.

(23) Pouvreau, M.; Greathouse, J. A.; Cygan, R. T.; Kalinichev, A. G. Structure of Hydrated Kaolinite Edge Surfaces: DFT Results and Further Development of the ClayFF Classical Force Field with Metal-O-H Angle Bending Terms. *Journal of Physical Chemistry C* **2019**, *123* (18), 11628–11638. https://doi.org/10.1021/acs.jpcc.9b00514.

(24) Pouvreau, M.; Greathouse, J. A.; Cygan, R. T.; Kalinichev, A. G. Structure of Hydrated Gibbsite and Brucite Edge Surfaces: DFT Results and Further Development of the ClayFF Classical Force Field with Metal-O-H Angle Bending Terms. *Journal of Physical Chemistry C* **2017**, *121* (27), 14757–14771. https://doi.org/10.1021/acs.jpcc.7b05362.

(25) Meleshyn, A.; Bunnenberg, C. Swelling of Na⁄Mg-Montmorillonites and Hydration of Interlayer Cations: A Monte Carlo Study. *The Journal of Chemical Physics* **2005**, *123* (7), 74706. https://doi.org/10.1063/1.2011392.

(26) Tester, C. C.; Aloni, S.; Gilbert, B.; Banfield, J. F. Short- and Long-Range Attractive Forces That Influence the Structure of Montmorillonite Osmotic Hydrates. *Langmuir* **2016**, *32* (46), 12039–12046. https://doi.org/10.1021/acs.langmuir.6b03265.

(27) Akinwunmi, B.; Hirvi, J. T.; Kasa, S.; Pakkanen, T. A. Swelling Pressure of Na- and Ca-Montmorillonites in Saline Environments: A Molecular Dynamics Study. *Chemical Physics* **2020**, *528*, 110511. https://doi.org/10.1016/j.chemphys.2019.110511.

(28) SAIYOURI, N.; TESSIER, D.; HICHER, P. Y. Experimental Study of Swelling in Unsaturated Compacted Clays. *Clay Minerals* **2004**, *39* (4), 469–479. https://doi.org/10.1180/0009855043940148.

(29) Rotenberg, B.; Morel, J.-P.; Marry, V.; Turq, P.; Morel-Desrosiers, N. On the Driving Force of Cation Exchange in Clays: Insights from Combined Microcalorimetry Experiments and Molecular Simulation. *Geochimica et Cosmochimica Acta* **2009**, *73* (14), 4034–4044. https://doi.org/https://doi.org/10.1016/j.gca.2009.04.012.

(30) Skipper, N. T.; Sposito, G.; Chang, F.-R. C. Monte Carlo Simulation of Interlayer Molecular Structure in Swelling Clay Minerals. 2. Monolayer Hydrates. *Clays and Clay Minerals* **1995**, *43* (3), 294–303. https://doi.org/10.1346/CCMN.1995.0430304.

(31) NORRISH, K. Crystalline Swelling of Montmorillonite: Manner of Swelling of Montmorillonite. *Nature* **1954**, *173* (4397), 256–257. https://doi.org/10.1038/173256a0.

(32) Yamada, H.; Nakazawa, H.; Hashizume, H.; Shimomura, S.; Watanabe, T. Hydration Behavior of Na-Smectite Crystals Synthesized at High Pressure and High Temperature. *Clays and Clay Minerals* **1994**, *42* (1), 77–80.

(33) Anderson, R. L.; Ratcliffe, I.; Greenwell, H. C.; Williams, P. A.; Cliffe, S.; Coveney, P. v. Clay Swelling — A Challenge in the Oilfield. *Earth-Science Reviews* **2010**, *98* (3), 201–216. https://doi.org/https://doi.org/10.1016/j.earscirev.2009.11.003.

(34) Morrow, C. P.; Yazaydin, A. Ö.; Krishnan, M.; Bowers, G. M.; Kalinichev, A. G.; Kirkpatrick, R. J. Structure, Energetics, and Dynamics of Smectite Clay Interlayer Hydration: Molecular Dynamics and Metadynamics Investigation of Na-Hectorite. *The Journal of Physical Chemistry C* **2013**, *117* (10), 5172–5187. https://doi.org/10.1021/jp312286g.

(35) Ferrage, E.; Lanson, B.; Sakharov, B. A.; Geoffroy, N.; Jacquot, E.; Drits, V. A. Investigation of Dioctahedral Smectite Hydration Properties by Modeling of X-Ray Diffraction Profiles: Influence of Layer Charge and Charge Location. *American Mineralogist* **2007**, *92* (10), 1731–1743. https://doi.org/doi:10.2138/am.2007.2273.

(36) Suter, J. L.; Coveney, P. v.; Anderson, R. L.; Greenwell, H. C.; Cliffe, S. Rule Based Design of Clay-Swelling Inhibitors. *Energy and Environmental Science* **2011**, *4* (11), 4572–4586. https://doi.org/10.1039/c1ee01280k.

(37) Makaremi, M.; Jordan, K. D.; Guthrie, G. D.; Myshakin, E. M. Multiphase Monte Carlo and Molecular Dynamics Simulations of Water and CO2 Intercalation in Montmorillonite and Beidellite. *The Journal of Physical Chemistry C* **2015**, *119* (27), 15112–15124. https://doi.org/10.1021/acs.jpcc.5b01754.

(38) Uddin, F. Clays, Nanoclays, and Montmorillonite Minerals. *Metallurgical and Materials Transactions A* **2008**, *39* (12), 2804–2814. https://doi.org/10.1007/s11661-008-9603-5.

For Table of Contents Only